A Modified Born-Infeld Model of Electrons and a Numerical Solution Procedure

Martin Kraus (kraus.martin@gmail.com)

February 29, 2024

Abstract

This work presents a modified Born-Infeld field theory and a numerical solution procedure to compute electron-like solutions of this field theory in the form of rotating waves of finite self-energy. For the well-known constants of real electrons, the computed solution results in a Born-Infeld parameter of 5×10^{22} V/m, which is consistent with previous work.

1 Introduction

About 90 years ago, Born and Infeld proposed a classical field theory, in which "particles of matter are considered as singularities of the field and mass is a derived notion to be expressed by field energy (electromagnetic mass)" [BIF34]. This led to the Born-Infeld model of electron-like particles without magnetic moment [BIF34]. Since these particles are represented by an electrostatic solution, they lack the internal clock hypothesized by de Broglie [dB25]. In previous works, I speculated that both shortcomings could be addressed by two independent modifications of Born-Infeld field theory [Kra23a, Kra23b].

This work combines these two modifications and proposes a numerical solution procedure for the resulting modified Born-Infeld field theory. Using this procedure, the Born-Infeld parameter is estimated to be 5×10^{22} V/m, which is consistent with the lower limit reported by Soff, Rafelski, and Greiner [SRG73].

The rest of this paper is organized as follows. Section 2 introduces the Lagrangian density and the corresponding field equations of the proposed model. Section 3 presents a numerical solution procedure to compute rotating wave solutions with a single peak. Section 4 describes the use of this procedure to compute the Born-Infeld parameter. Section 5 discusses results and future work, while Section 6 concludes this article.

2 Modified Born-Infeld Field Theory

This work employs the International System of Units (SI), basic Ricci calculus including Einstein summation convention, and the Minkowski metric tensor η in the form $\mathrm{diag}(+1, -1, -1, -1)$. More details about the notation are provided in previous work [Kra23a].

Compared to the Lagrangian density proposed by Born and Infeld [BIF34, Equation 2.11], the Lagrangian density $\mathscr{L}(A_\nu, \partial_\mu A_\nu)$ of the proposed model includes two previously proposed modifications [Kra23a, Kra23b], such that it becomes:

$$\mathscr{L}(A_\nu, \partial_\mu A_\nu) \stackrel{\text{def}}{=} \sqrt{1 - \frac{1}{b^2}(\partial^\mu A^\nu)(\partial_\mu A_\nu)} - 1 \tag{1}$$

with the four-potential $(A^0, A^1, A^2, A^3) \stackrel{\text{def}}{=} (\phi/c, A_x, A_y, A_z)$ and the Born-Infeld parameter b, which specifies a maximum field strength of the magnetic field $\mathbf{B} = \nabla \times \mathbf{A}$ and electric field $\mathbf{E}/c = -\frac{\partial}{\partial t}\mathbf{A}/c - \nabla\phi/c$.

The Euler-Lagrange equations are then:

$$0 = \partial_\mu \left(\frac{\partial \mathscr{L}(A_\nu, \partial_\mu A_\nu)}{\partial\left(\partial_\mu A_\nu\right)} \right) - \frac{\partial \mathscr{L}(A_\nu, \partial_\mu A_\nu)}{\partial A_\nu} = \partial_\mu \frac{-1}{b^2} \frac{\partial^\mu A^\nu}{\sqrt{1 - \frac{1}{b^2}(\partial^\alpha A^\beta)(\partial_\alpha A_\beta)}}. \tag{2}$$

Thus:

$$0 = \partial_\mu \frac{\partial^\mu A^\nu}{\sqrt{1 - \frac{1}{b^2}(\partial^\alpha A^\beta)(\partial_\alpha A_\beta)}} \qquad \text{with } \nu = 0, \ldots, 3. \tag{3}$$

3 Numerical Solution Procedure

The main motivation for the proposed Lagrangian is that it allows for a solution that for large distances approximates the electric and magnetic fields of an electron, includes a peak of the field values that is rotating with an electron's Compton frequency on a circle of the radius of an electron's reduced Compton wavelength, and features a total field energy equal to the rest mass energy of an electron. In order to compute this solution, specific values for all constants (including the Born-Infeld parameter), appropriate boundary conditions (including the position of and field values at the peak), and an appropriate time-dependency of all fields (letting the peak move at the speed of light on a circular orbit) are assumed.

Due to these assumptions, the predictive power of the proposed model is unclear. (The only "prediction" in this work is the computation of the Born-Infeld parameter reported in Section 4; arguably this is not a prediction of an observable quantity.) However, the model is considered valuable even without predictive power since it allows to study a classical field theory that not only models classical features of electrons but also quantum mechanical features such as their Compton frequency.

On the most abstract level, the proposed numerical procedure is a hierarchical partial differential equation solver that first computes a field solution on a coarse 128^3 grid that covers the peak's orbit, and then interpolates the resulting solution to obtain boundary values that are used to solve the same partial differential equation on a finer 128^3 grid that represents a volume that is 4^3-times smaller than the volume covered by the coarser grid and is centered around the peak of the solution. This refinement step is repeated five times such that the full hierarchical grid includes six 128^3 grid levels at different resolutions.

Each grid level includes 128^3 grid points with three 16-bit floating-point numbers representing the A^0, A^1, and A^2 components of the four-potential (the A^3 component is assumed to be 0 as its direction is orthogonal to the rotation plane) and one 16-bit floating-point number representing the denominator $a \stackrel{\text{def}}{=} \sqrt{1 - (\partial^\alpha A^\beta)(\partial_\alpha A_\beta)/b^2}$. In the current implementation on a graphics processing unit, each 128^3 grid level is represented by two 2048×1024 floating-point render textures such that all grid points of one grid level may be processed in parallel by ping-pong rendering between two render textures while boundary values may be computed by filtered look-ups in a render texture of the next coarser grid level. Since the field solution is assumed to rotate around the center of the coarsest grid level, time dependencies are not explicitly represented in the grid. Instead, only a three-dimensional "frozen" solution is stored in memory, and time derivatives are approximated with central differences by sampling a grid level at appropriately rotated positions. Spatial derivatives are approximated with central differences between neighboring grid points.

On each hierarchy level, solutions are improved iteratively using a Jacobi method with a few thousand iterations until the solution has converged sufficiently. Figure 1 visualizes a slice of a solution for $A^0 = \phi/c$ on the coarsest grid level.

Apart from steps for initialization, visualization, and tracking of convergence, each iteration consists of the following four steps for all relevant grid points:

1. setting boundary values
2. filtering field values
3. approximating the denominator $a \stackrel{\text{def}}{=} \sqrt{1 - (\partial^\alpha A^\beta)(\partial_\alpha A_\beta)/b^2}$
4. computing new field values with a single Jacobi iteration

Each step is discussed in detail in the following sections.

3.1 Setting Boundary Values

The boundary of each 128^3 grid level consists of the grid point where the peak is located, four neighboring grid points, and all grid points at a distance of 61 grid units or more from the center of the grid

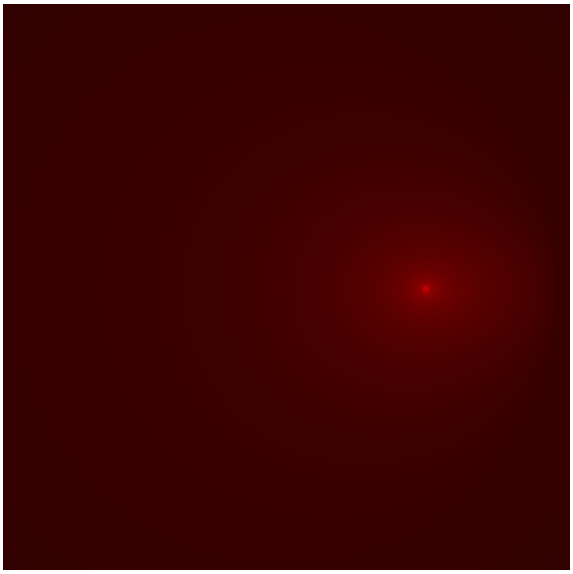

Figure 1: Visual representation of the electric potential $A^0 = \phi/c$ on the slice of the coarsest 128^3 grid level including the (invisible) rotation center in the center of the image and the off-center peak to the right of the center.

level. (The grid unit Δx is the distance in meters between the positions represented by two neighboring grid points.) For the latter grid points on the coarsest grid level, $\mathbf{A}$ is set to $\mathbf{0}$ and ϕ is set based on a Coulomb potential. For these grid points on finer grid levels, all field values are set based on values interpolated from the field values near the corresponding position on the next coarser grid level.

On the coarsest grid level, the peak is located on the x-axis halfway between the center of the grid and the edge of the grid. This position determines the value of the grid unit Δx, which is given by the reduced Compton wavelength of electrons divided by the number of grid points between the peak and the center of the grid, which is also the rotation center of the field solution. On finer grid levels, the peak is located at the center of the grid level.

On the coarsest grid level, ϕ at the peak is set to 1 and the units of ϕ are scaled such that a Coulomb potential for an elementary charge is reproduced at the boundary. On finer grid levels, by default, the value of ϕ at the grid level's peak is multiplied with 4 compared to the next coarser grid level in order to reproduce a Coulomb potential on all grid levels. However, there is an additional scaling of ϕ on the finest levels as explained in the next paragraph.

The vector potential $\mathbf{A}$ is set to $\mathbf{0}$ at the grid point (i, j, k) of the peak. At the four neighboring grid points in the i, j-plane, $\mathbf{A}$ is set to form a vortex, i.e., at the $(i-1, j, k)$ grid point, $\mathbf{A}$ is set to point in the positive j direction; at the $(i, j+1, k)$ grid point, $\mathbf{A}$ is set to point in the positive i direction; at the $(i+1, j, k)$, $\mathbf{A}$ is set to point in the negative j direction; and at the $(i, j-1, k)$ grid point, $\mathbf{A}$ is set to point in the negative i direction. The magnitude of $\mathbf{A}$ on the coarsest grid level is chosen such that the solution at large distances approximates the magnetic dipole field of an electron. On finer grid levels, by default, the magnitude of $\mathbf{A}$ is multiplied with 16 compared to the next coarser grid level in order to reproduce a dipole field on all grid levels. If, however, the resulting magnitude of $\mathbf{A}$ divided by the grid unit Δx of a grid level is greater than the Born-Infeld parameter b (the maximum field strength), then the magnitude of $\mathbf{A}$ is set to $b \times \Delta x$. Compared to the default value, this may be considered a scaling with a factor less than 1. The same scaling factor is applied to the default value of ϕ at the peak position.

Limiting values of the four-potential at the peak to $b \times \Delta x$ ensures that field strengths near the peak may reach values up to b but not beyond. Notably, it also results in decreasing(!) values of the components of the four-potential at the peak for sufficiently high grid levels as their grid unit Δx decreases for increasing level, which (in the limit of infinitely high grid levels) avoids discontinuities of the field at the peak.

3.2 Filtering Field Values

After boundary values have been set, a $3 \times 3 \times 3$ triangular kernel filter is applied to the field values of all grid points. The purpose of this filter is to prevent cases where successive Jacobi iterations spread and/or magnify discretization errors. Additionally, it helps distributing field energy that is injected

at the peak position by the boundary condition. Furthermore, it tends to reduce field strengths near the peak (which is numerically beneficial, in particular for the computation in the next step) without lowering the maximum peak value of the four-potential that the solution may potentially reach.

3.3 Approximating the Denominator *a*

This step computes for each grid point (i, j, k) the denominator $a \stackrel{\text{def}}{=} \sqrt{1 - (\partial^\alpha A^\beta)(\partial_\alpha A_\beta)/b^2}$, which appears in the field equations (see Section 2) and stores the result for use in the next step. Values less than 0.01 are replaced by 0.01 to prevent spreading of numerical errors. In terms of the electric potential ϕ and the magnetic vector potential $\mathbf{A}$, the denominator $a = a(\phi, \mathbf{A})$ is given by:

$$a(\phi, \mathbf{A}) = \sqrt{1 - \frac{1}{b^2}\left(\left(\frac{1}{c}\frac{\partial}{\partial t}\phi/c\right)^2 - (\nabla\phi/c)^2 - \left(\frac{1}{c}\frac{\partial}{\partial t}\mathbf{A}\right)^2 + (\nabla A_x)^2 + (\nabla A_y)^2 + (\nabla A_z)^2\right)} \tag{4}$$

As mentioned above, spatial derivatives are approximated with central differences between neighboring grid points, for example:

$$\frac{\partial}{\partial x}A_y(i, j, k) \approx \frac{1}{2\Delta x}\left(A_y(i + 1, j, k) - A_y(i - 1, j, k)\right). \tag{5}$$

Time derivatives are approximated with central differences by sampling appropriately rotated positions (assuming that the field solution is rotating with the peak moving at the speed of light). If the position rotated backward in time (by Δt)[1] is denoted by $(i_{-\Delta t}, j_{-\Delta t}, k_{-\Delta t})$, then the future value of ϕ at (i, j, k) after Δt depends on the value of ϕ (in the "frozen" field) at the backward rotated position, i.e., the future value at (i, j, k) is given by $\phi(i_{-\Delta t}, j_{-\Delta t}, k_{-\Delta t})$ (which rotates onto the position (i, j, k) after Δt). The vector-valued field $\mathbf{A}$ presents the additional complication that the field value has to be forward rotated itself, which may be specified with a rotation matrix $\mathrm{R}_{+\Delta t}$. Thus, the future value of $\mathbf{A}$ after Δt is $\mathrm{R}_{+\Delta t}\mathbf{A}(i_{-\Delta t}, j_{-\Delta t}, k_{-\Delta t})$. The past values are computed analogously with $-\Delta t$ instead of $+\Delta t$ and vice versa. With these expressions, the time-derivative of, for example, A_y reads:

$$\frac{\partial}{\partial t}A_y(i, j, k) \approx \frac{1}{2\Delta t}\big((\mathrm{R}_{+\Delta t}\mathbf{A}(i_{-\Delta t}, j_{-\Delta t}, k_{-\Delta t}))_y - (\mathrm{R}_{-\Delta t}\mathbf{A}(i_{+\Delta t}, j_{+\Delta t}, k_{+\Delta t}))_y\big). \tag{6}$$

3.4 Computing New Field Values with a Single Jacobi Iteration

As mentioned above, the field equations (see Section 2) are solved using an iterative Jacobi method. To this end, each field equation is discretized and solved for one of the components of the four-potential at a specific grid position (i, j, k). As an example, the field equation

$$0 = \partial_\mu \frac{\partial^\mu A^\nu}{\sqrt{1 - \frac{1}{b^2}(\partial^\alpha A^\beta)(\partial_\alpha A_\beta)}} \tag{7}$$

for $\nu = 2$ is considered, which is solved for $A^2(i, j, k) = A_y(i, j, k)$. (The other field equations are treated completely analogously.) In terms of the electric potential ϕ and the magnetic vector potential $\mathbf{A}$, the equation for $\nu = 2$ reads:

$$0 = \frac{1}{c}\frac{\partial}{\partial t}\frac{\frac{1}{c}\frac{\partial}{\partial t}A_y}{a(\phi, \mathbf{A})} - \frac{\partial}{\partial x}\frac{\frac{\partial}{\partial x}A_y}{a(\phi, \mathbf{A})} - \frac{\partial}{\partial y}\frac{\frac{\partial}{\partial y}A_y}{a(\phi, \mathbf{A})} - \frac{\partial}{\partial z}\frac{\frac{\partial}{\partial z}A_y}{a(\phi, \mathbf{A})} \tag{8}$$

Derivatives are discretized using finite differences between neighboring grid points. $a(\phi, \mathbf{A})$ is approximated by the arithmetic mean of the values at those neighboring grid points. For example, one

[1] The actual value of Δt is chosen such that the peak is moved by the rotation approximately by one grid unit Δx and all other points are rotated by the same angle; except for the coarsest level, where the value of Δt is doubled in order to improve the method's robustness.

of the four terms on the right-hand side is approximated this way:

$$\frac{\partial}{\partial x}\frac{\frac{\partial}{\partial x}A_y}{a(\phi,\mathbf{A})} \approx \frac{1}{\Delta x}\left(\frac{(A_y(i+1,j,k)-A_y(i,j,k))/\Delta x}{(a(i+1,j,k)+a(i,j,k))/2} - \frac{(A_y(i,j,k)-A_y(i-1,j,k))/\Delta x}{(a(i,j,k)+a(i-1,j,k))/2}\right) \quad (9)$$

$$= \Big((A_y(i+1,j,k)-A_y(i,j,k))\,(a(i,j,k)+a(i-1,j,k))\,/2 \quad (10)$$
$$- \,(A_y(i,j,k)-A_y(i-1,j,k))\,(a(i+1,j,k)+a(i,j,k))\,/2\Big)$$
$$/\ \big(\Delta x^2(a(i+1,j,k)+a(i,j,k))(a(i,j,k)+a(i-1,j,k))/4\big)$$

$$= \Big(-A_y(i,j,k)\,(a(i-1,j,k)+2a(i,j,k)+a(i+1,j,k))\,/2 \quad (11)$$
$$+ A_y(i+1,j,k)\,(a(i,j,k)+a(i-1,j,k))\,/2$$
$$+ A_y(i-1,j,k)\,(a(i+1,j,k)+a(i,j,k))\,/2\Big)$$
$$/\ \big(\Delta x^2(a(i+1,j,k)+a(i,j,k))(a(i,j,k)+a(i-1,j,k))/4\big)$$

$$\approx \Big(-2a(i,j,k)A_y(i,j,k) + A_y(i+1,j,k)\,(a(i,j,k)+a(i-1,j,k))\,/2 \quad (12)$$
$$+ A_y(i-1,j,k)\,(a(i+1,j,k)+a(i,j,k))\,/2\Big)$$
$$/\ \big(\Delta x^2(a(i+1,j,k)+a(i,j,k))(a(i,j,k)+a(i-1,j,k))/4\big)$$

Approximating all four terms on the right-hand side of the field equation analogously results in this approximation:

$$0 = \frac{1}{c}\frac{\partial}{\partial t}\frac{\frac{1}{c}\frac{\partial}{\partial t}A_y}{a(\phi,\mathbf{A})} - \frac{\partial}{\partial x}\frac{\frac{\partial}{\partial x}A_y}{a(\phi,\mathbf{A})} - \frac{\partial}{\partial y}\frac{\frac{\partial}{\partial y}A_y}{a(\phi,\mathbf{A})} - \frac{\partial}{\partial z}\frac{\frac{\partial}{\partial z}A_y}{a(\phi,\mathbf{A})} \quad (13)$$

$$\approx \Big(-2a(i,j,k)A_y(i,j,k) \quad (14)$$
$$+ (\mathrm{R}_{+\Delta t}\mathbf{A}(i_{-\Delta t},j_{-\Delta t},k_{-\Delta t}))_y\,(a(i,j,k)+a(i_{+\Delta t},j_{+\Delta t},k_{+\Delta t}))\,/2$$
$$+ (\mathrm{R}_{-\Delta t}\mathbf{A}(i_{+\Delta t},j_{+\Delta t},k_{+\Delta t}))_y\,(a(i_{-\Delta t},j_{-\Delta t},k_{-\Delta t})+a(i,j,k))\,/2\Big)$$
$$/\ \big(c^2\Delta t^2(a(i_{-\Delta t},j_{-\Delta t},k_{-\Delta t})+a(i,j,k))(a(i,j,k)+a(i_{+\Delta t},j_{+\Delta t},k_{+\Delta t}))/4\big)$$
$$- \Big(-2a(i,j,k)A_y(i,j,k) + A_y(i+1,j,k)\,(a(i,j,k)+a(i-1,j,k))\,/2$$
$$+ A_y(i-1,j,k)\,(a(i+1,j,k)+a(i,j,k))\,/2\Big)$$
$$/\ \big(\Delta x^2(a(i+1,j,k)+a(i,j,k))(a(i,j,k)+a(i-1,j,k))/4\big)$$
$$- \Big(-2a(i,j,k)A_y(i,j,k) + A_y(i,j+1,k)\,(a(i,j,k)+a(i,j-1,k))\,/2$$
$$+ A_y(i,j-1,k)\,(a(i,j+1,k)+a(i,j,k))\,/2\Big)$$
$$/\ \big(\Delta x^2(a(i,j+1,k)+a(i,j,k))(a(i,j,k)+a(i,j-1,k))/4\big)$$
$$- \Big(-2a(i,j,k)A_y(i,j,k) + A_y(i,j,k+1)\,(a(i,j,k)+a(i,j,k-1))\,/2$$
$$+ A_y(i,j,k-1)\,(a(i,j,k+1)+a(i,j,k))\,/2\Big)$$
$$/\ \big(\Delta x^2(a(i,j,k+1)+a(i,j,k))(a(i,j,k)+a(i,j,k-1))/4\big)$$

In order to apply the Jacobi method, this equation is solved for $A_y(i,j,k)$, which results in:

$$
\begin{aligned}
A_y(i,j,k) \;\approx\; & \Bigg(\Big(\big(\mathrm{R}_{+\Delta t}\mathbf{A}(i_{-\Delta t}, j_{-\Delta t}, k_{-\Delta t})\big)_y \left(a(i,j,k) + a(i_{+\Delta t}, j_{+\Delta t}, k_{+\Delta t})\right)/2 \\
& + \big(\mathrm{R}_{-\Delta t}\mathbf{A}(i_{+\Delta t}, j_{+\Delta t}, k_{+\Delta t})\big)_y \left(a(i_{-\Delta t}, j_{-\Delta t}, k_{-\Delta t}) + a(i,j,k)\right)/2 \Big) \\
& / \left(c^2\Delta t^2 (a(i_{-\Delta t}, j_{-\Delta t}, k_{-\Delta t}) + a(i,j,k))(a(i,j,k) + a(i_{+\Delta t}, j_{+\Delta t}, k_{+\Delta t}))/4\right) \\
& - \Big(A_y(i+1,j,k)\left(a(i,j,k) + a(i-1,j,k)\right)/2 \\
& + A_y(i-1,j,k)\left(a(i+1,j,k) + a(i,j,k)\right)/2 \Big) \\
& / \left(\Delta x^2 (a(i+1,j,k) + a(i,j,k))(a(i,j,k) + a(i-1,j,k))/4\right) \\
& - \Big(A_y(i,j+1,k)\left(a(i,j,k) + a(i,j-1,k)\right)/2 \\
& + A_y(i,j-1,k)\left(a(i,j+1,k) + a(i,j,k)\right)/2 \Big) \\
& / \left(\Delta x^2 (a(i,j+1,k) + a(i,j,k))(a(i,j,k) + a(i,j-1,k))/4\right) \\
& - \Big(A_y(i,j,k+1)\left(a(i,j,k) + a(i,j,k-1)\right)/2 \\
& + A_y(i,j,k-1)\left(a(i,j,k+1) + a(i,j,k)\right)/2 \Big) \\
& / \left(\Delta x^2 (a(i,j,k+1) + a(i,j,k))(a(i,j,k) + a(i,j,k-1))/4\right) \Bigg) \\
& \Big/ \Bigg(2a(i,j,k) \\
& / \left(c^2\Delta t^2 (a(i_{-\Delta t}, j_{-\Delta t}, k_{-\Delta t}) + a(i,j,k))(a(i,j,k) + a(i_{+\Delta t}, j_{+\Delta t}, k_{+\Delta t}))/4\right) \\
& - 2a(i,j,k)/\left(\Delta x^2 (a(i+1,j,k) + a(i,j,k))(a(i,j,k) + a(i-1,j,k))/4\right) \\
& - 2a(i,j,k)/\left(\Delta x^2 (a(i,j+1,k) + a(i,j,k))(a(i,j,k) + a(i,j-1,k))/4\right) \\
& - 2a(i,j,k)/\left(\Delta x^2 (a(i,j,k+1) + a(i,j,k))(a(i,j,k) + a(i,j,k-1))/4\right) \Bigg)
\end{aligned}
\tag{15}
$$

The field equations for $\nu = 0$, 1, and 3 result in analogous equations for $\phi(i,j,k)$, $A_x(i,j,k)$, and $A_z(i,j,k)$.

An individual step of a naive Jacobi method consists of applying these equations to compute new values for $\phi(i,j,k)$ and $\mathbf{A}(i,j,k)$ at all grid points. While this method is certainly not the most efficient method to solve the field equations, it is (in the technical sense) embarrassingly parallel and, therefore, very well suited for a straightforward implementation on graphics processing units.

4 Determining the Born-Infeld Parameter

Like other versions of Born-Infeld field theory, the proposed model includes a Born-Infeld parameter b, which (in this work) specifies the maximum field strength of the magnetic field and the maximum field strength of the electric field divided by c. For easier comparison with previous work, however, the numeric value is specified in V/m, which is the value of $b \times c$, i.e., the maximum field strength of the electric field.

Determining the Born-Infeld parameter b is particularly interesting because all other constants of the model (electric charge, magnetic moment, and Compton frequency of an electron as well as speed of light) are well known constants of nature. As in previous work [BIF34], b is chosen such that the total field energy of the field solution equals the rest mass energy of an electron. To this end, the field's energy density u is assumed to be given by

$$
u \stackrel{\text{def}}{=} \frac{1}{2}\Big(\varepsilon_0 |\mathbf{E}|^2 + \frac{1}{\mu_0}|\mathbf{B}|^2\Big) \tag{16}
$$

with the vacuum permittivity ε_0, vacuum permeability μ_0, electric field strength $\mathbf{E} = -\partial/\partial t\mathbf{A} - \nabla\phi$, and magnetic field strength $\mathbf{B} = \nabla \times \mathbf{A}$.

In order to compute the total field energy of a field solution for a given value of parameter b, the energy density $u = u(i, j, k)$ is computed for each grid point (i, j, k) of all grid levels and multiplied by the volume Δx^3 represented by each grid point. The resulting energy contributions are summed except for grid points that are covered by finer grid levels in order to avoid double counting. (The energy of the corresponding volume of the finest grid level is estimated based on the energy density at its boundary; but the energy contribution of the finest grid level is negligible in any case.) The field energy in the volume outside the coarsest grid level is estimated as one quarter of the energy of the coarsest grid level (which turns out to be less than 1% of the total field energy).

The resulting total field energy is compared to the well-known rest mass energy of an electron, and the parameter b is adjusted iteratively until the two energies match. This fitting process resulted in a value of 5×10^{22} V/m for $b \times c$, which is consistent with (i.e., greater than) the lower limit reported by Soff, Rafelski, and Greiner [SRG73]. However, it should be noted that there are still various potential sources of systematic errors; thus, the reported value should be considered an initial result that has to be improved in future work.

5 Discussion and Future Work

The presented model of electrons features the same long-range electric and magnetic fields, and the same Compton frequency as real electrons, as well as a field energy equal to the rest mass energy of real electrons. In this sense, the model appears to constitute a substantial improvement over the original model by Born and Infeld [BIF34]. Since the presented model leads to a numeric solution of the field equations, many questions about the model may be studied by analyzing this numeric solution instead of analyzing non-linear, non-separable field equations. While an analysis of the numeric solution cannot replace an analysis of the field equations, it certainly may help forming hypotheses and testing them for plausibility. Many of these questions relate to emerging features of the model, e.g., whether a Lorentz-like force exists in the model; whether the Compton frequency is predicted by the model; whether the model predicts a Bohr-Sommerfeld-like quantization condition; whether other solutions of the field equations exist (for the same Born-Infeld parameter) that correspond to other charged leptons; etc.

6 Conclusion

This work presents a modified Born-Infeld field theory and a numerical solution procedure, which was successfully used to compute field solutions that may serve as models of electrons with realistic electric charge, magnetic dipole moment, and Compton frequency. Furthermore, the proposed procedure was used to adjust the Born-Infeld parameter such that the total field energy of the solution matches the rest mass energy of electrons. The model raises many questions that might lead to a deeper understanding of real electrons and quantum physics in general. Perhaps the presented model might even provide new meaning to a quote by Richard Feynman from his answer to a question about the possibility of future alternatives to quantum electrodynamics: "If it's going to be any kind of a model, it's going to be at least as weird as this thing [i.e., quantum electrodynamics]" [Fey79].

References

[BIF34] Max Born, Leopold Infeld, and Ralph Howard Fowler. Foundations of the new field theory. *Proceedings of the Royal Society of London. Series A, Containing Papers of a Mathematical and Physical Character*, 144(852):425–451, 1934.

[dB25] Louis de Broglie. Recherches sur la théorie des Quanta. *Annales de Physique*, 10(3):22–128, January 1925. English translation by A. F. Kracklauer.

[Fey79] Richard Feynman. Photons: Corpuscles of light. Sir Douglas Robb Memorial Lectures at The University of Auckland, 1979.

[Kra23a] Martin Kraus. A modified Born-Infeld model of electrons as rotating waves. viXra:2304.0046, 2023.

[Kra23b] Martin Kraus. A modified Born-Infeld model of electrons with realistic magnetic dipole moment. viXra:2311.0081, 2023.

[SRG73] Gerhard Soff, Johann Rafelski, and Walter Greiner. Lower bound to limiting fields in nonlinear electrodynamics. *Phys. Rev. A*, 7:903–907, Mar 1973.

A Revisions

- Original version submitted to vixra.org on December 28, 2023.
- Revision February 29, 2024: Fixed Equation (16) and its description; clarified notation in Equations (5) and (6); added footnote [1] on page 4; added ∂'s in Equation (2).